Development of an active truss element for control of precision structures

Eric H. Anderson
Donald M. Moore, MEMBER SPIE
James L. Fanson
Jet Propulsion Laboratory
California Institute of Technology
4800 Oak Grove Drive
Pasadena, California 91109

Mark A. Ealey, MEMBER SPIE
Litton/Itek Optical Systems
10 Maguire Road
Lexington, Massachusetts 02173-3199

Abstract. An active structural element for use in precision control of large space structures is described. The *active member* is intended to replace a passive strut in a truss-like structure. It incorporates an eddy current displacement sensor and an actuator that is either piezoelectric (PZT) or electrostrictive (PMN). The design of the device is summarized. Performance of separate PZT and PMN actuators is compared for several properties relevant to submicrometer control of precision structures.

Subject terms: active optical components; active structures; active strut; piezoelectricity; electrostriction; structural control.

Optical Engineering 29(11), 1333-1341 (November 1990).

CONTENTS

1. INTRODUCTION

The performance of future large precision optical systems such as orbiting interferometers[1] and segmented mirror telescopes[2] will depend directly on the alignment and stability of optical components attached to large lightweight structural frameworks. Displacements of micrometers from a nominal configuration may either limit the resolution of the instruments or render data from observations useless. Active structures technology is being developed by the Jet Propulsion Laboratory to produce high performance structures that make use of a limited number of active structural members to control elastic motion at the submicrometer level.

In a typical active truss structure, a small percentage of the struts are replaced by *active members*.[3] The active member described in this paper is a structural component that includes an eddy current displacement sensor and an actuator that exploits either piezoelectricity or electrostriction to provide strain due to an electrical input. Both forms of electromechanical coupling are commonly used to provide mechanical actuation. Piezoceramic lead zirconate titanate (PZT) actuators have been employed for micropositioning of precision machinery and optics[4] and have been extensively used for mirror wavefront control in adaptive optics.[5-7] Itek has used an electrostrictive material, lead magnesium niobate (PMN), for the last decade in adaptive optics applications. There is also current interest in using both actuation methods in many types of microdevices.[8]

At JPL, two truss structures have been constructed that make use of active members with piezoelectric motor elements and built-in displacement sensors (Kaman Constant Length Strut, or CLS), as well as a simple member containing an actuator only (Burleigh PZL-150). A load cell is normally placed in series with the active members for use with the displacement sensor in collocated control. Active damping experiments incorporating several control methodologies have been done on both testbeds.[9,10] Recently, robust H_∞ and μ synthesis control have been demonstrated on the Precision Truss structure,[11] and control with two active members has been implemented on a 12 m truss aboard a KC-135 aircraft that experiences brief periods of microgravity.

The goal of the current effort is to develop a component that will meet the necessary structural and control requirements of space science missions involving large precision structures. The eventual space application drives the design toward low mass, high linearity, reliability, and temporal and thermal stability.

An active member is shown in Fig. 1. It has a diameter of 27 mm, a total length of 173 mm, and a mass of 190 or 240 g, depending on the actuator motor used. For the precision applications envisioned, where large strokes or forces are not required, the easily controlled electrically coupled materials—piezoelectrics and electrostrictives—were chosen. A magnetostrictive actuator motor is currently being developed for later incorporation.

Invited paper AD-104 received March 20, 1990; revised manuscript received July 20, 1990; accepted for publication July 23, 1990.

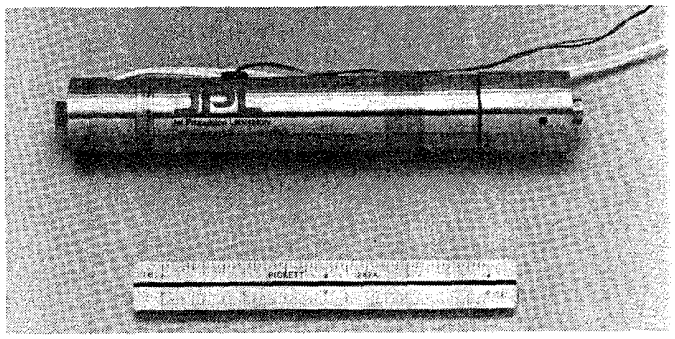

Fig. 1. JPL active member.

The active member was evaluated as a device down to the nanometer displacement level. The design allows incorporation and evaluation of different actuator motors. A comparison was made of two candidate actuator materials (piezoelectric and electrostrictive) with respect to stroke and force capability, linearity, bandwidth, and temporal and thermal stability. Electrostrictive actuation has been extensively employed by Itek but has seen little application in structural control. The tests carried out show significant advantages over the more common piezoceramics in temporal stability and repeatability, at the expense of properties that are fairly temperature sensitive. The candidate actuation methods are currently being evaluated for application at typical mission temperatures in high earth orbit (near 100 K).

In this paper the relevant properties of the piezoelectric and electrostrictive ceramics used in the actuator motors are first reviewed. Then the design specifications and rationale are described and the performance of the active members using the two separate actuators is detailed. Comparisons of capacitance, bandwidth, power consumption, frequency response, throw, force, hysteresis, creep, and thermal stability are made. Finally, the nanometer level mechanical performance of the assembled active member is reviewed.

2. PROPERTIES OF PIEZOELECTRIC AND ELECTROSTRICTIVE CERAMICS

Both piezoelectricity and electrostriction are phenomena characterized by a coupling between mechanical and electrical properties. From the standpoint of incorporation into a structural model or structural control system based on strain actuation, they may be treated similarly. That is, they output a certain elastic quantity (strain or stress) per unit of electrical input (typically voltage). However, there are significant differences in material properties that complicate the electromechanical coupling and may become important in specific applications and actuator implementations.

The full electromechanical relations necessary for an accurate description of induced strain actuation in piezoceramics include an electrical relation, a mechanical relation, and a coupling term.[12] For piezoceramic materials such as lead zirconate titanate, the relation between actuation strain and applied electric field is

$$S = \begin{bmatrix} 0 & 0 & 0 & 0 & d_{15} & 0 \\ 0 & 0 & 0 & d_{15} & 0 & 0 \\ d_{31} & d_{31} & d_{33} & 0 & 0 & 0 \end{bmatrix}^t \begin{bmatrix} E_1 \\ E_2 \\ E_3 \end{bmatrix} , \tag{1}$$

where the superscript t indicates transpose. The d_{33} coefficient is exploited in the current active member design, by stacking 70 wafers, each 1 mm in thickness. Based on Eq. (1), a stress-free actuator will deliver a displacement of

$$\Delta \ell = N \ell d_{33} \frac{V}{t} , \tag{2}$$

where ℓ is the actuator length, N is the number of wafers, V is the applied voltage, and t is the thickness of each wafer.

For electrostrictive materials such as lead magnesium niobate, the electrostrictive coefficient (m) matrix analogous to Eq. (1) is

$$S = \begin{bmatrix} m_{33} & m_{31} & m_{31} & 0 & 0 & 0 \\ m_{31} & m_{33} & m_{31} & 0 & 0 & 0 \\ m_{31} & m_{31} & m_{33} & 0 & 0 & 0 \end{bmatrix}^t \begin{bmatrix} E_1^2 \\ E_2^2 \\ E_3^2 \end{bmatrix} . \tag{3}$$

A stacked electrostrictive actuator using m_{33} will deliver a displacement of

$$\Delta \ell = N \ell m_{33} \frac{V^2}{t} . \tag{4}$$

The longitudinal piezoelectric strain coefficient in terms of the electrostriction coefficient is by definition

$$d_{33} = \left(\frac{\delta S_3}{\delta E_3} \right)_T = 2 m_{33} E_3 , \tag{5}$$

that is, the strain per field increases linearly with field.

Typical PZT and PMN materials exhibit high stiffness and can provide essentially constant gain (mechanical output/electrical input) for a given field up to several kilohertz. Neither material type is, however, accurately modeled by a single constant coefficient (d_{33} or m_{33}). The d_{33} and m_{33} coefficients actually change as the dielectric coefficient is altered with increased mechanical deformation:

$$d_{33} \propto \varepsilon_{33}^T , \quad m_{33} \propto (\varepsilon_{33}^T)^2 . \tag{6}$$

This property is discussed elsewhere.[13] The dependence of the piezoelectric strain coefficient d on ε is particularly troublesome in piezoceramics. Not only does the dielectric coefficient change in magnitude (typically by a factor of 2 over an actuator operating range), but the dielectric loss tangent can be as high as 20% to 30%. This loss tangent increases with higher strains. Thus, the effective displacement per volt from a piezoceramic actuator stack will change (increase) at larger mechanical displacements. In addition, the relation is increasingly hysteretic with amplitude. Closely related to hysteresis is the phenomenon of piezoelectric creep. The step response of a piezoelectric actuator to an applied field will show an increasing displacement over time. Aging of piezoceramics also occurs, leading to a slow degradation of properties. In addition, the lossy dielectric coefficient causes piezoelectric actuators to suffer from capacitive heating, a phenomenon that becomes increasingly important as the frequency of operation is increased.

Electrostrictives also have a variable dielectric coefficient, which, however, decreases with strain, causing strain that is less than quadratic with field. The departure from quadratic behavior is often beneficial since the field-strain relation "turns over" and creates a sizable nearly linear region. Loss tangents are typically low (near 1%), implying low hysteresis, negligible creep, and little aging. Because of their high coefficients (near

20,000 compared to 1500 for a typical piezoceramic), electrostrictive actuators have higher capacitances, implying lower actuator bandwidth for a fixed current. Capacitive heating is, however, greatly reduced.

3. MECHANICAL DESIGN AND DESCRIPTION

3.1. Initial Specifications and Requirements

Work on control of active truss structures was in its infancy at JPL when the decision was made to construct a zero-stiction precision active member. In lieu of a firm design requirement, the active member design team arbitrated the following strawman specifications: overall length < 8 in. (200 mm); nominal diameter 1 in. (25 mm); zero displacement force > 100 lb (450 N); zero force displacement ± 1 mil (± 25 μm); displacement sensing range ± 4 mils (± 100 μm); displacement sensing resolution 1 μin. (25 nm); stiction zero.

The zero-stiction requirement, and to a lesser extent the desire to have high resolution displacement sensing capability, represented the challenge to the design team and set the active member discussed here apart from other available devices. The JPL design draws many features from the Kaman CLS (U.S. Patent 4,742,261), including the high resolution displacement sensing capability. The CLS was originally intended for accurate positioning of optical components, achieved through operation in a closed loop mode. When used as a structural load-bearing member, it exhibits a small amount of stiction.

3.2. Design philosophy

The overriding design challenge was the production of a zero-stiction active member configuration providing absolute fidelity of commanded and measured motion. The way this was met will be discussed. In addition, the rationale for the choice of a displacement measuring system is explained and other structural, materials, and fabrication considerations are addressed.

In the current active member (Fig. 2), the actuator motor is isolated from all bending moments by cross-blade flexures at both ends of the actuator. Blade flexures were chosen over rod flexures since they are stiffer axially for the same degree of moment isolation. Collocation of the cross-blades minimizes their total axial length. The output stem of the actuator motor assembly is supported on a pair of flexures: a diaphragm flexure and a wide blade flexure. This flexure pair, termed "parallel motion flexures," offers zero frictional resistance to the actuator motor even though side loads and bending moments may be applied to the output stem.

The desire to eliminate the stick-slip characteristics of Belleville springs, the availability of the wire electrical discharge machining (EDM) technique, and the ease of analysis led to the unusual configuration of the motor preloading spring. Precipitation hardening stainless steel was chosen over titanium for this spring for a long fatigue life.

Titanium alloy Ti-6Al-4V was chosen for nearly all structural components, primarily because of its relatively low coefficient of thermal expansion among the nonexotic structural metals. Additionally, titanium offers relatively high specific strength and stiffness. Notable exceptions are the actuator motor, aluminum crush washers, motion sensors, aluminum sensor target, and stainless steel preload spring.

3.3. Description

The zero-stiction precision active member may be thought of as two distinct and separable assemblies both functionally and physically. The actuator motor assembly produces axial motion and the motion sensor assembly measures axial displacement.

Figures 2 and 3 illustrate the major actuator components. From the left end of the actuator motor assembly they are the dead end cross-blade flexure, crush washer, motor centering pilot, actuator motor, a second pilot, crush washer, live end cross-blade flexure, and parallel motion flexures. These are all held in place in a tubular barrel by a tubular cap attached by lens-type screw threads. A preload spring and preload adjusting nut are added at the live end to provide the desired compressive preload on the actuator motor.

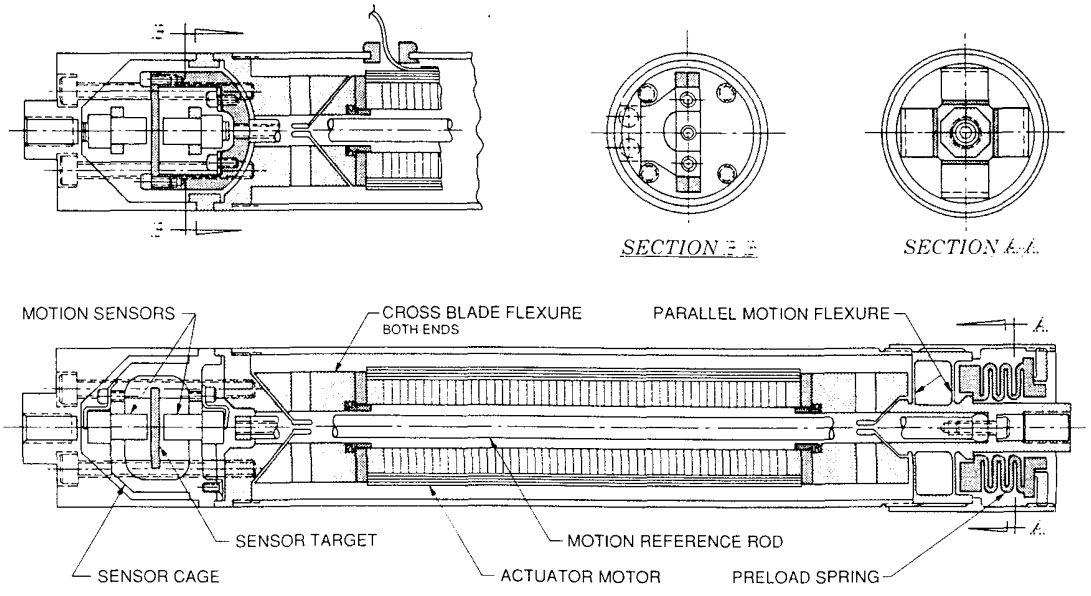

Fig. 2. Schematic of active member.

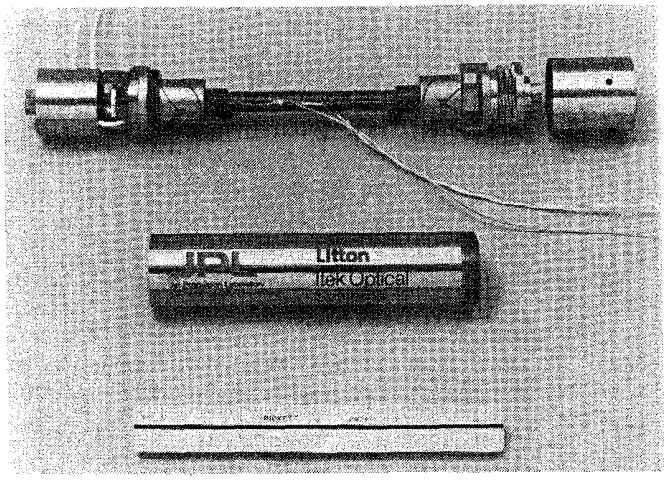

Fig. 3. Active member with electrostrictive actuator motor.

The sensor assembly provides a measurement of the displacement of the live end with respect to the dead end of the active member. The motion sensors are mounted at the dead end (left end in Fig. 2) of the actuator and the displacement at the live end is transferred by a motion reference rod. This rod is attached to the live end stem, passing through the actuator motor assembly, and is attached to the motion sensor target via a target yoke. The yoke passes through a cage that holds the differential eddy current proximity sensors and positions the target midway between these two sensors. It is flexure-supported from the sensor cage.

Integration of the motion sensor assembly and the actuator motor assembly is accomplished by clamping the sensor cage to the dead end of the actuator motor assembly by means of the dead end cap and four socket head screws. The live end of the reference rod is attached to the live end output stem by a single socket head screw.

The final assembly step is to calibrate the internal displacement sensor using a laser interferometer with a precision of 1.25 nm. The sensor was linear to within 0.2% over the full actuator displacement range with the active members mechanically unconstrained.

4. ACTIVE MEMBER DEVICE PERFORMANCE

In this section, the performance of the PZT and PMN active members is described. The tests illustrate the strengths and weaknesses of both the active member as a device and of the two separate actuator motors. The capabilities of the active members are summarized in Table I. The specifications are quoted for the assembled devices, not the actuators alone. All tests were carried out at room temperature (≈22°C).

5. ELECTRICAL INPUTS

For different reasons, both the PZT and PMN active members were operated with a dc bias voltage. A large field applied against the polarization direction of a piezoceramic (shrinking the stack) can partially or fully depole the material. Repeated application of any field opposite to the poling direction causes a degradation or loss of piezoelectric properties. The bias field aligned with the polarization allows operation from 0 to a maximum voltage.

The displacement of the PMN is independent of the direction of the applied field, so an input voltage centered about 0 V is not useful. The nearly linear region of the PMN field-strain curve lies away from 0 field where the relation is purely quadratic. If the bias voltage is in the middle of the range, a reasonably linear output can be expected. The upper voltage limit for both actuators is set by arcing between layers. For the PZT the limit is 1000 V (or a field of 1000 V/mm) and for the PMN the limit is 300 V (1700 V/mm) because of better manufacturing.

TABLE I. Active member specifications.

Property	PZT[1]	PMN
Stiffness (short circuit)	14.6 N/μm (83.6 lb/mil)	9.75 N/μm (55.7 lb/mil)
Mass	240 g (0.53 lb)	190 g (0.42 lb)
Maximum Operating Voltage	1000 V	300 V
Normal Bias Voltage	500 V	150 V
Single Wafer Thickness	1.0 mm (39.4 mils)	0.18 mm (7.0 mils)
Displacement (1 Hz)	63.4 μm (2.50 mils)	39.5 μm (1.56 mils)
Force (1 Hz)	505 N (114 lb)	455 N (102 lb)
Hysteresis (1 Hz)[2]	16.0 %	1.2 %
Capacitance (25 Hz)[2]	0.6 μF	7.6 μF
Current, rms (25 Hz)[2]	33 mA	127 mA
Temperature Sensitivity	n. a.	1.2% /°C

[1] Average of 2 members
[2] For maximum displacement

6. CAPACITANCE, BANDWIDTH, AND POWER CONSUMPTION

When viewed from an electrical standpoint, piezoelectric and electrostrictive ceramics are simply capacitors with additional electromechanical properties. The variable capacitance with mechanical displacement leads to nonlinearities, which will be illustrated. When using an active member, the actuator capacitance sets amplifier current requirements. For a fixed amplifier current limit, the device capacitance establishes a bandwidth or cutoff frequency above which the amplifier applies reduced voltage:

$$f_c = \frac{1}{2\pi} \frac{I_{\text{lim}}}{CV_{op}} . \tag{7}$$

The bandwidth is thus higher for lower operating voltage. To achieve high bandwidth with as small an amplifier as possible, it is desirable to keep the actuator capacitance low. A stacked actuator consists of a number N of individual wafers that are electrically in parallel and have total capacitance

$$C = \frac{N\varepsilon A}{t} , \tag{8}$$

where t is one wafer thickness and A is the cross-sectional area. For a given stroke, the voltage necessary to provide a certain field can be reduced by making the actuators as thin as possible.

However, this will cause the capacitance to increase quadratically because of the increased number of wafers as well as the reduced thickness of each layer. The area must be high to satisfy device stiffness, throw, and force requirements. The dielectric coefficient is a material property that cannot be changed. Typically, PMN has a coefficient near 15,000 (i.e., 15,000 times the "permittivity of free space" ε_o), and PZT near 1,500.

The dielectric coefficient is not constant for either PMN or PZT. This leads to a capacitance that changes with magnitude. The thickness change due to material deformation is *not* responsible for a significant capacitance change. To quantify the changing capacitance, both voltage and current must be measured. A standard test involves application of a single frequency sinusoidal input voltage at different amplitudes added to a bias voltage. The current is then measured and the capacitance determined by Eq. (7).

The measured capacitance is plotted in Fig. 4 as a function of displacement amplitude for a single frequency test at 25 Hz. The scale on the PMN plot is 10 times higher than that on the PZT plot in order to show the difference in capacitances. This difference is accentuated by the thinner wafers and higher dielectric coefficient, and reduced by the lower area. The larger capacitance has a direct bearing on the active member bandwidth.

The PZT data show a capacitance that increases steadily with amplitude, by roughly a factor of 2 over the full displacement range. This implies a higher current consumption at large displacements of the member and will strongly affect the gain of the member (i.e., the displacement output per volt input). The PMN curve shows reduced capacitance at low displacement. A portion of this effect is due to measurement error.

The actuator capacitance directly affects power consumption, and although it is minimal, large amplifiers are required. Even a perfect capacitor has a current requirement, which increases proportionally to frequency and voltage. Thus, the amplifier must deliver both high voltage to induce large displacements and high current to maintain high bandwidth. The voltage and current capacity of the amplifier represent instantaneous requirements, not power consumption. The actual power consumed goes into capacitive heating and, to a much lesser extent, mechanical losses. The power consumed is proportional to the dielectric loss tangent $\tan\delta$. Thus, because the PZT loss tangent is greater, the piezoelectric actuator consumes more power than the electrostrictor for a given voltage and current. The power consumption is easily estimated:

$$P = VI\tan\delta = \omega CV^2\tan\delta \ . \tag{9}$$

For full-out operation at maximum voltage, at 25 Hz, the PZT active member consumes 3.77 W and the PMN active member consumes 1.33 W (based on an assumed loss tangent of 5%).

The effect of capacitive heating on performance of the actuators is a concern. Because of the construction of the PZT stacks as delivered, it was not possible to mount a thermocouple. The PMN thermocouple showed that under a steady state operating voltage of 75 ± 75 V at 100 Hz, the temperature increased between 2°C and 3°C, representing a 3% to 4% change in gain. Since more heat is generated by the piezoelectric, a larger temperature increase is expected. The actual temperature change depends on the heat exchange between components within the member. Capacitive heating may be important in future cryogenic applications.

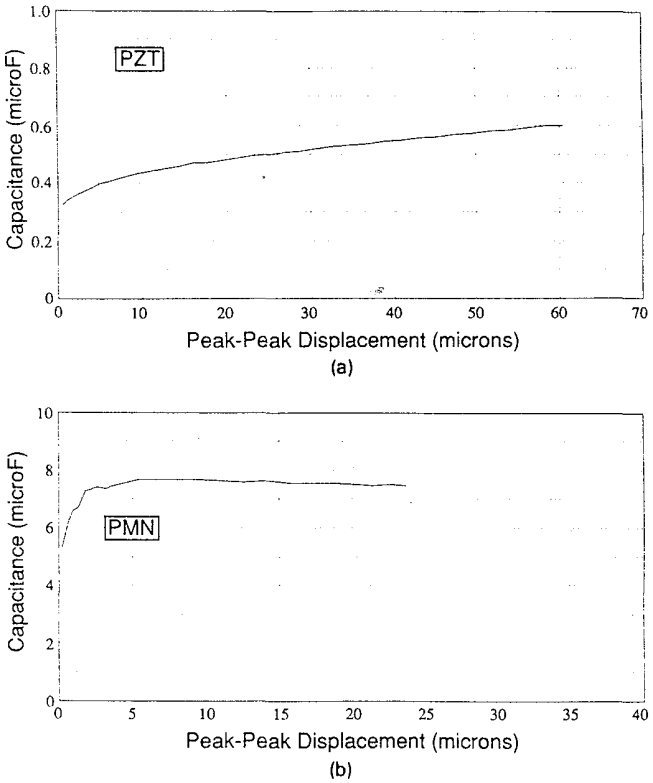

Fig. 4. Active member capacitance.

The variable dielectric coefficient that directly affects the capacitance is an important property of both PZT and PMN. Its effect will be apparent in many of the displacement-based data that follow.

7. FREQUENCY RESPONSE

The desired frequency response (displacement/volt) of the active member is flat, with no dynamics over frequency and constant (nominally zero) phase. The magnitude and phase of the two PZT and one PMN active member are shown in Fig. 5. The standard sine sweep test represents application of identical bias fields (500 V/mm) and alternating fields (100 V/mm) to both actuators. The relatively low ac voltages of the sweep kept the current low and minimized the effect of amplifier rolloff.

The gain (magnitude) plot [Fig. 5(a)] illustrates that both actuator types give nearly constant output over the frequency range shown. The gain for the PMN member is greater only because the actuator is composed of thinner wafers, meaning that a higher electric field is achieved for the same voltage.

The PMN member magnitude drops 2.6% between 1 and 100 Hz. The PZT member gains drop by 6.7% and 6.0%. The stronger frequency dependence in the PZT is due to the effect of creep at low frequency.

The only actuator dynamics below 1 kHz are due to bending in the internal reference rod. This is barely observable from the differential sensors, showing up as a less than 10° phase change. The reference rod bending frequency was 680 Hz, 660 Hz, and 570 Hz for the three active members.

The phase plot illustrates the effect of the lossy dielectric coefficient in PZT. The phase lag is greatest at low frequencies, where the loss tangent is largest.

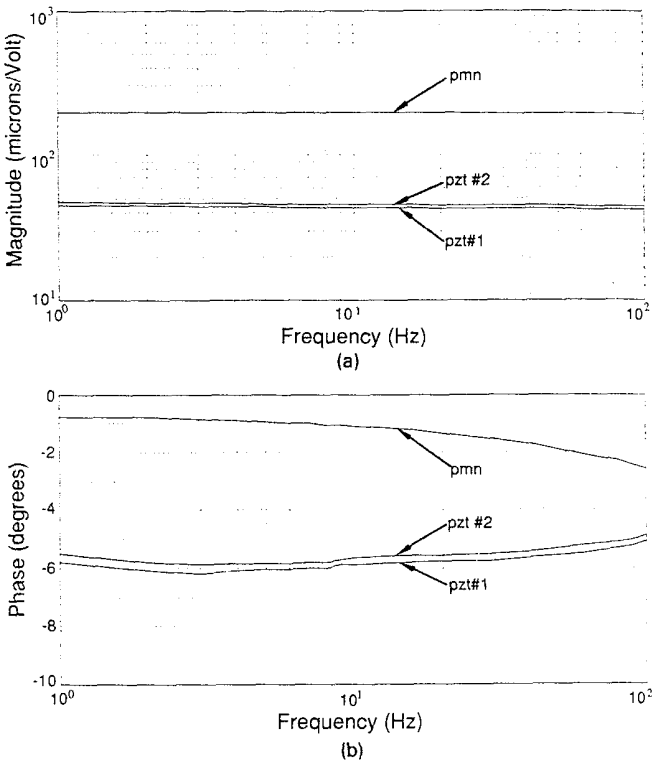

Fig. 5. Active member transfer functions.

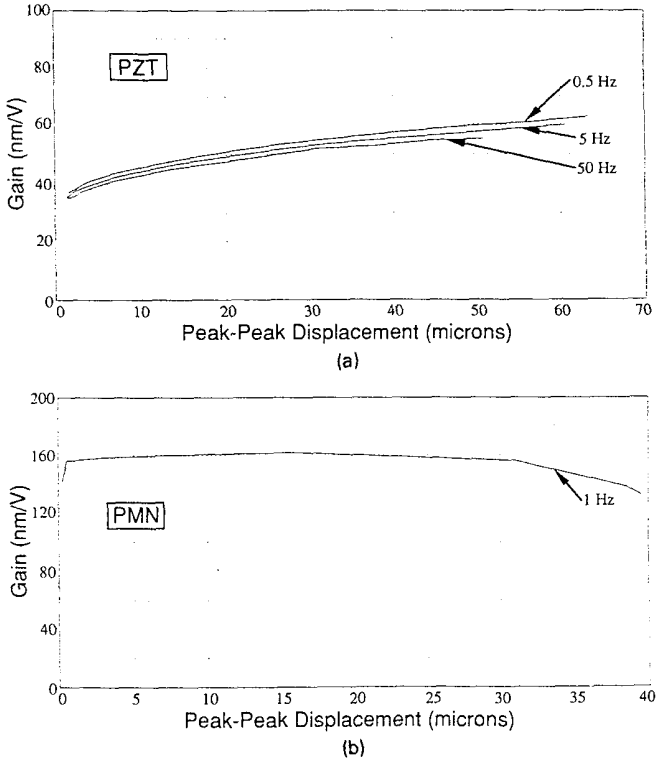

Fig. 6. Active member gains.

8. GAIN

Although the transfer functions are nearly constant with frequency, there is a significant dependence of gain on displacement amplitude for both actuator types. In this series of tests, time histories of voltage and displacement were recorded for various amplitudes at several different frequencies. The gain is computed by dividing the peak-peak displacement by the peak-peak voltage applied, with the results plotted in Fig. 6.

The PMN data show little change from 1 to 100 Hz (as seen in Fig. 5). Again, the overall level of the PMN gain is higher because a higher electric field is enforced for a given voltage. The PZT gain shows an increase with amplitude. This dependence on displacement level is nearly identical to the capacitance-displacement plot of Fig. 4. The PMN gain is nearly constant with amplitude and only drops off for high peak-peak displacements, where the total voltage swings from 0 to 300 V. At zero voltage, the gain is zero [Eq. (5)]. The change in the PZT active member gain with frequency is more readily apparent.

The gain at zero displacement is multiplied by the input voltage and member stiffness to determine device blocked force capability.

The increased gain in the piezoelectric active member can be troublesome in control design. To simplify design, an approximation must be made that sets a fixed gain. The increasing gain with amplitude is undesirable since the actual gain margin will be reduced from that predicted. The slight decrease in PMN gain at high amplitudes may actually be beneficial in limiting the control authority slightly for large amplitudes.

9. HYSTERESIS

The effect of the lossy dielectric coefficient is seen clearly in a plot of the applied voltage and displacement over one cycle. The same plot illustrates the basic field-strain relations. The displacement due to a 1 Hz sinusoidal voltage input plotted against the total voltage is shown in Fig. 7. As expected, the PZT active member locus is not a straight line, and the PMN locus is not a perfect parabola.

The plot corresponding to the PZT active member [Fig. 7(a)] shows three hysteresis loops at three different input voltages. The gain plotted in Fig. 6 represents the slope of the hysteresis curves. For larger amplitudes, the slope increases, implying a larger gain. In addition, the aspect ratio of the loops (or the percent hysteresis) increases. This quantity is defined as the maximum displacement width of the loop divided by the peak-peak displacement. The three loops pictured have 16.6%, 15.4%, and 13.8% hysteresis. Hysteresis appears as a phase lag in the transfer function representation (Fig. 5).

Figure 7(b) displays the shape of the PMN actuator output. A single curve is shown. An applied voltage from 100 to 200 V, for example, would follow the same curve, with a barely discernible difference at the lower end. Near zero voltage, the curve is nearly parabolic. As the voltage is increased, the curve flattens out before the slope decreases further at higher voltage. The gain shown in Fig. 6 represents the peak-peak displacement divided by the peak-peak voltage. The hysteresis is small (1.2%) and limited mainly to a region between 0 V and the bias voltage. This low hysteresis is reflected in the small phase lag shown in Fig. 5.

Hysteresis can be detrimental to active control. An actuator with inherent hysteresis requires control effort that may reduce control authority elsewhere. The hysteresis is potentially harmful at dc, where it can cause residual displacements.

10. STEP RESPONSE AND CREEP

The step response is a useful test of system dynamics. For the active member, the step response illustrates the quick response

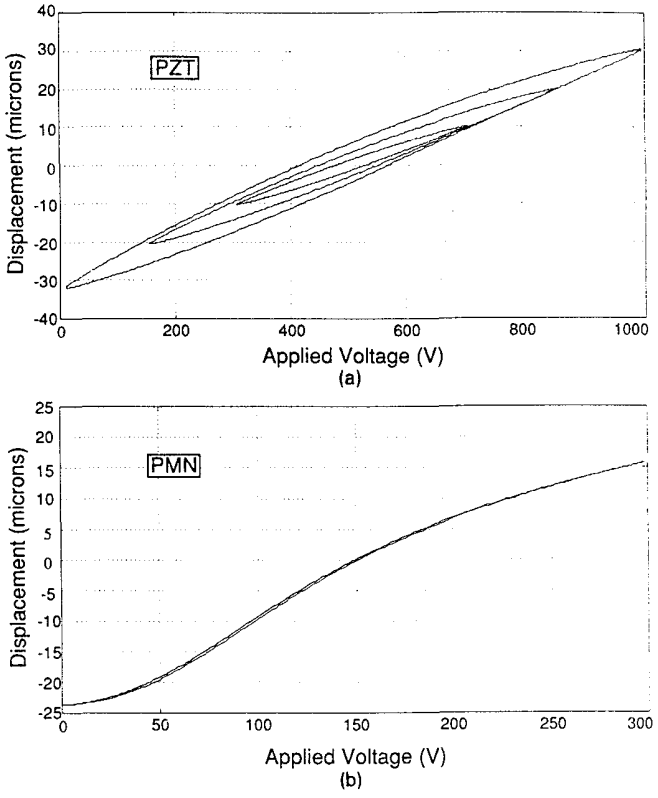

Fig. 7. Active member hysteresis.

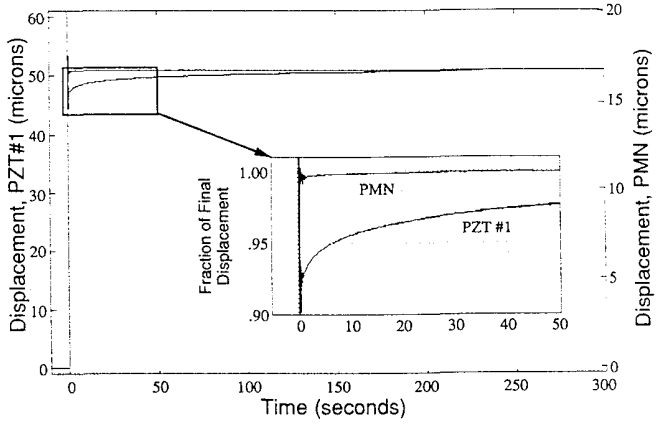

Fig. 8. Active member step response, illustrating creep.

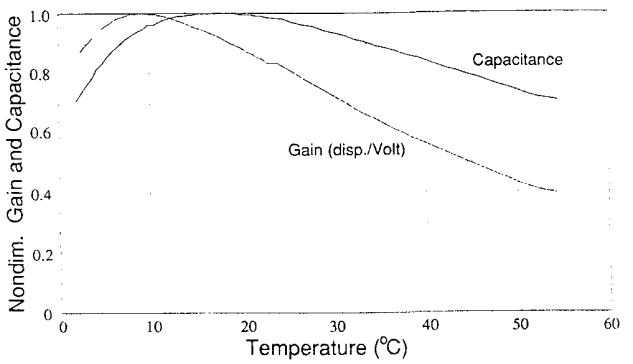

Fig. 9. Temperature variation of PMN properties.

of both the PZT and PMN actuation schemes, as well as creep in the PZT actuation.

A set of tests was conducted in which a step voltage was applied to the active members. In Fig. 8, the results of two separate tests are shown. In one test, a 700 V step was applied to the PZT member. In a second, a 125 V step was applied to the PMN member. Because of the difference in wafer thicknesses, the applied field was identical (700 V/mm) for the two tests. For convenience, the two plots are scaled to the same asymptotic level.

The initial response shows ringing introduced by an imperfect voltage switch. Both actuators have response times better than 1 ms. The expanded plot showing the first 50 s after the step illustrates the strong creep in the PZT, as well as limited creep in the PMN. Although the electric field goes from 0 to a constant voltage, there is a lag in the corresponding polarization change. As the physical material is deformed, dipoles are moved such that the polarization increases.

The PZT member has reached only 93% of its final value 2 s after the step, while the PMN member has reached 99.5% of its final value. The amount of relative creep is comparable to the relative hysteresis in the two members. Creep is not a significant problem for vibration control.

It is possible to significantly reduce both hysteresis and creep in PZT by employing "charge control." By commanding a charge to the actuator, the effect of the lossy dielectric coefficient in the charge voltage relation is avoided, and a displacement directly proportional to the input is achieved. Enforcing charge is more difficult than simple voltage control but can be accomplished by employing a standard technique.[14]

11. TEMPERATURE DEPENDENCE OF PMN

Temperature dependence of the active member properties is also of interest. The present goal is to evaluate the actuator in a temperature range around the typical ground-based structural control testbed condition. The test conducted represents a first cut at understanding the thermal characteristics of the active member. In the final performance test, the effect of temperature on the PMN actuator was measured. A thermocouple was placed on the PMN actuator based on an expected change of 4%/°C in gain near room temperature. The PMN actuator was biased with 100 V and a 25 V 0-peak signal was input at 50 Hz. At room temperature, the active member has a gain of roughly 160 nm/V (Fig. 6).

The entire active member was heated to 55°C in an oven, then allowed to cool to room temperature with a constant voltage input. The rms current and displacement were recorded. The member was then placed in a refrigerator and allowed to cool to 2°C while the voltage was applied and the current and displacement recorded. The displacement sensors are believed to be accurate within 2% over the entire temperature range. Handling of the active member between the elevated and reduced temperature phase of the testing caused a small anomaly in the data at room temperature.

The test results are shown in Fig. 9. The maximum gain occurred at 9°C, where it exceeded the room temperature value by 20%. This temperature corresponds to the Curie temperature of the PMN material. The gain at 55°C was down 60% from the maximum. The measured capacitance (based on the current) peaked at 17°C. Both quantities dropped off sharply at lower temperatures.

The change in gain at room temperature was about 1.2%/°C, considerably lower than expected. In the future, a comprehensive evaluation of the actuators will be carried out in the application temperature ranges. The gain change per degree as well as the total expected temperature excursion will determine the significance of the temperature dependence. A recent study investigated gain and hysteresis in PMN over a temperature range from −50°C to 100°C.[15]

As a byproduct of the limited thermal testing, the effective member coefficient of thermal expansion (CTE) was calculated to be 5.6×10^{-6}/°C. This value is slightly larger than expected, in part because a steel reference rod was used.

12. OVERALL DEVICE PRECISION

The JPL active member was designed to eliminate the stiction exhibited by commercially available actuators that were not intended for use as primary structure. A series of comparison tests were therefore conducted on both the JPL design and the Kaman CLS.

Stiction caused by the interaction of the actuator motor assembly with the actuator housing was investigated through a simple self-loading test. The member was mounted at one end on an inclinometer fixture and rotated by up to 90°. The outer housing was then tapped to "break loose" any stuck components. The member was then returned to its initial position, where the displacement was recorded. The member was again tapped, and the displacement recorded. The difference was attributed to stiction. A single nanometer was discernible in the displacement sensor output.

Based on a series of tests, this type of stiction was found to be no greater than 1 nm in the JPL active member. Further quantification was not possible due to the resolution of the sensor. Because of the sensitivity of its sensors to cable movement, it was not possible to obtain accurate data on the Kaman CLS.

In a second set of tests, the active member was mounted vertically in series with a dc load cell. Compressive and tensile loads ranging from −60 to +75 N were applied for 1 to 2 s and then released. The load and displacement were recorded prior to, during, and subsequent to the loading event. The data were later analyzed to determine the amount of residual displacement remaining after the return to zero load.

Typically, the residual displacements in the Kaman CLS and JPL active member were 10 to 100 nm and 1 to 10 nm, respectively. The maximum residual displacements were 270 and 30 nm, respectively. The residual displacements for the two active members are plotted against the one-time load in Fig. 10. Since the two active members have different stiffnesses, the displacements are normalized to the corresponding peak displacement values (at peak load) and expressed as a percent. The compressive loading data are shown as negative to indicate a negative displacement, although the residual displacement divided by the peak displacement gives a positive number. The scatter in the data indicates the sensitivity of the phenomenon. It is clear, however, that the current active member is an order of magnitude better than the Kaman CLS in this series of tests.

Both active members were found to exhibit a "bedding in" phenomenon. That is, while an initial loading of 50 N might produce 25 nm of nonrecoverable displacement, five consecutive loadings of 50 N would produce 25 nm, 5 nm, 0 nm, 0 nm, and 0 nm. If a set of compressive loads was then applied, displacements were typically 35 nm, 10 nm, 0 nm, 0 nm, and 0 nm. A repeat of five tension loads would produce similar results.

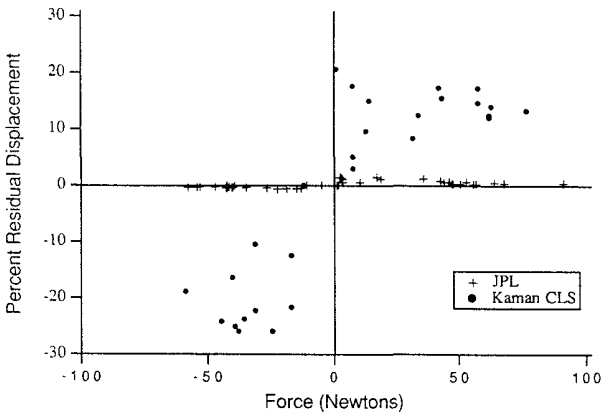

Fig. 10. Nonrecoverable displacement in the Kaman CLS and JPL active member.

Thus, there is inelastic behavior in the active members, which for the loads tested is roughly 250 nm in the Kaman CLS and 25 nm in the JPL active member. The total inelastic displacement appears to increase with load, while the percent residual displacement is roughly constant for small peak displacements.

In the case of the JPL active member the above noted inelastic behavior cannot be attributed to stiction. In the case of the Kaman CLS, it almost certainly includes stiction. This inelastic behavior has caused us to reconsider our prejudice that preloaded joints behave elastically. In the 100 nm range they do not. If this inelastic joint behavior becomes a problem, a critical look at joint design will be necessary.

13. FUTURE WORK

The current active member has met the original design specifications and is suitable for current ground-based active structure testbeds. Other induced strain actuation mechanisms such as magnetostriction are planned for future devices, as are new methods for measuring collocated displacement and force. Flight qualification of the device and optimization of performance in the cryogenic temperature regime are also planned.

14. ACKNOWLEDGMENTS

The research described in this paper was carried out by the Jet Propulsion Laboratory, California Institute of Technology, under a contract with the National Aeronautics and Space Administration. The authors would like to express their appreciation for the contributions of the following individuals: R. Bamford, G. Blackwood, P. Bruneau, J. Hendrickson, J. O'Brien, W. Schmitigal, D. Thornton, E. Verret at JPL, and P. Davis at Itek.

15. REFERENCES

1. R. Laskin and M. San Martin, "Spaceborne imaging interferometer—the JPL CSI mission focus," in *Third NASA/DOD Controls Structures Interaction Technology Conference Proc.* (1989).
2. P. N. Swanson, J. B. Breckinridge, A. Diner, R. E. Freeland, W. R. Irace, P. M. McElroy, A. B. Meinel, and A. F. Tolivar, "System concept for a moderate cost large deployable reflector," Opt. Eng. 25(9), 1045–1054 (1986).
3. J. L. Fanson, E. H. Anderson, and D. Rapp, "Active structures for use in precision control of large optical systems," Opt. Eng. 29(11) (1990).
4. M. A. Ealey, "Precision electrodisplacive microactuators," in *Precision Engineering and Optomechanics*, Proc. SPIE 1167, 85–102 (1989).
5. M. A. Ealey and J. Wellman, "Fundamentals of deformable mirror design and analysis," in *Precision Engineering and Optomechanics*, Proc. SPIE 1167, 66–84 (1989).
6. D. Chiarappa and C. Claysmith, "Deformable mirror surface control techniques," J. Guidance and Control 4(1), 27–34 (1981).

7. J. Hardy, "Instrumental limitations in adaptive optics for astronomy," in *Active Telescope Systems*, F. Roddier, ed., Proc. SPIE 1114, 2–13 (1989).
8. E. Cross, "Piezoelectric and electrostrictive sensors and actuators for adaptive structures and smart materials," in *Adaptive Structures*, ASME AD-Vol. 15 (1989).
9. J. Fanson, G. Blackwood, and C. Chu, "Active member control of precision structures," in *30th AIAA SDM Conf. Proc.*, AIAA Paper 89-1329 (1989).
10. G. Chen and B. Lurie, "Frequency domain analysis for active damping augmentation," in *31st AIAA SDM Dynamics Specialists Conf. Proc.*, AIAA Paper 90-1243 (1990).
11. J. Fanson, C. Chu, R. Smith, and E. Anderson, "Active member control of a precision structure with an H_∞ performance objective," in *31st AIAA SDM Dynamics Specialists Conf. Proc.*, AIAA Paper 90-1224 (1990).
12. "IEEE standard on piezoelectricity," ANSI/IEEE Std. 176-1987 (1987).
13. E. Anderson, D. Moore, J. Fanson, and M. Ealey, "Development of an active member using piezoelectric and electrostrictive actuation for control of precision structures," in *31st AIAA SDM Conf. Proc.*, AIAA Paper 90-1085 (1990).
14. R. Comstock, "Charge control of piezoelectric actuators to reduce hysteresis effects," U.S. Patent 4,263,527, Draper Labs., Cambridge, Mass.
15. G. Blackwood and F. Fleming, "Characterization of transverse field-induced strain in PMN:BA electroceramic plates," MIT Space Engineering Research Ctr. Rept. 7-90 (1990).

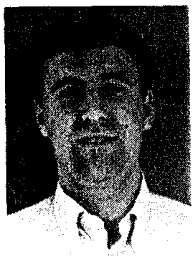

Eric Anderson received his SB and SM degrees from the Massachusetts Institute of Technology in 1986 and 1989. His master's thesis involved piezoceramics in active beam and plate structures. He has worked in the Structures Technology Group at Sikorsky Aircraft. He was recently employed in the control/structures interaction program at the Jet Propulsion Laboratory and is now a doctoral candidate at the MIT Space Engineering Research Center. He is currently conducting experiments on a tetrahedral truss testbed based on a design for a 30 m baseline space-based interferometer.

Donald Moore earned a BS degree in naval architecture at Webb Institute in 1962 and an MS degree in mechanical engineering design from Loyola Marymount University in 1977. Prior to joining JPL in 1972 he played key roles in the mechanical design of a hovercraft, rocket sleds, precision force measuring systems, special test apparatus, and an artificial rain field. At JPL he has maintained his interest in mechanical design, designing large conical spacecraft antennas utilizing knitted metallic reflecting surfaces, hail impact testing apparatus, innovative fasteners for tank tracks, and a six-axis dynamometer for characterizing the vibration of Stirling-cycle coolers. Occasionally, he has delved into somewhat more esoteric areas, doing extensive work on glass breakage and interconnect fatigue while in the terrestrial photovoltaics program.

James Fanson received his BS degree from the University of Wisconsin and his MS and Ph.D. degrees in 1982 and 1987 from the California Institute of Technology. He has participated in the design of an instrument optical bench for the Hubble Space Telescope and analyzed launch dynamics of the Galileo spacecraft. He is currently the lead engineer for active structures at JPL and the active structures element manager for the Control/Structure Interaction (CSI) program. He has been especially interested in the application of active structures technology to flight programs that require precision structural performance.

Mark A. Ealey: Biography and photograph appear with the paper "Standard SELECT electrostrictive lead magnesium niobate actuators for active and adaptive optical components" in this issue.